An Automatic Equalizer Based on Forward–Flyback Converter for Series-Connected Battery Strings

Yunlong Shang, *Student Member, IEEE*, Bing Xia, *Student Member, IEEE*, Chenghui Zhang, *Member, IEEE*, Naxin Cui, *Member, IEEE*, Jufeng Yang, *Student Member, IEEE*, and Chunting Chris Mi, *Fellow, IEEE*

***Abstract*—This paper proposes an automatic any-cells-to-any-cells battery equalizer, which merges the forward and flyback converters through a common multiwinding transformer. The windings of the transformer are divided into two groups, which have opposite polarities. The principles of the proposed equalizer are that the equalization in one group is achieved based on forward conversion and the balancing between the two different groups is based on flyback conversion, by which the magnetic energy stored in the transformer can be automatically reset without using additional demagnetizing circuits. Moreover, only one MOSFET and one primary winding are required for each cell, resulting in smaller size and lower cost. One pair of complementary control signals is employed for all MOSFETs, and energy can be automatically and directly delivered from any high-voltage cells to any low-voltage cells without the requirement of cell monitoring circuits, thereby leading to a high balancing efficiency and speed. The proposed topology can achieve the global equalization for a long battery string through connecting the secondary sides of transformers without the need of additional components for the equalization among modules, which also overcomes the mismatching problem of multiple windings. The validity of the proposed equalizer is verified through experiments, and the balancing efficiency can reach up to 89.4% over a wide range of conditions.**

***Index Terms*—Electric vehicles, equalizers, flyback conversion, forward conversion, lithium batteries, multiwinding transformers.**

Manuscript received September 6, 2016; revised November 29, 2016; accepted December 17, 2016. Date of publication February 24, 2017; date of current version June 9, 2017. This work was supported in part by the Major Scientific Instrument Development Program of the National Natural Science Foundation of China under Grant 61527809, in part by the National Natural Science Foundation of China under Grant 61633015 and Grant 61273097, in part by the Key Research and Development Program of Shandong Province under Grant 2016ZDJS03A02, in part by Nanjing Golden Dragon Bus Co., Ltd., and in part by the U.S. Department of Energy under the Graduate Automotive Technology Education Center Program.

Y. Shang is with the School of Control Science and Engineering, Shandong University, Shandong 250061, China, and also with the Department of Electrical and Computer Engineering, San Diego State University, San Diego, CA 92182 USA (e-mail: shangyunlong@mail.sdu.edu.cn).

B. Xia is with the Department of Electrical and Computer Engineering, San Diego State University, San Diego, CA 92182 USA, and also with the Department of Electrical and Computer Engineering, University of California, San Diego, CA 92093 USA (e-mail: bixia@eng.ucsd.edu).

C. Zhang and N. Cui are with the School of Control Science and Engineering, Shandong University, Jinan 250061, China (e-mail: zchui@sdu.edu.cn; cuinx@sdu.edu.cn).

J. Yang is with the Department of Electrical Engineering, Nanjing University of Aeronautics and Astronautics, Nanjing 211106, China, and also with the Department of Electrical and Computer Engineering, San Diego State University, San Diego, CA 92182 USA (e-mail: jufeng.yang@mail.sdsu.edu).

C. C. Mi is with the Department of Electrical and Computer Engineering, San Diego State University, San Diego, CA 92182 USA (e-mail: cmi@sdsu.edu).

Color versions of one or more of the figures in this paper are available online at http://ieeexplore.ieee.org.

Digital Object Identifier 10.1109/TIE.2017.2674617

I. Introduction

As ONE of the most widespread rechargeable batteries, the lithium-ion battery is widely used in many fields, e.g., electric vehicles, because of its low self-discharge rate, high cell voltage, efficient charging, no memory effect, and high energy density [1]–[3]. Many cells are connected in series–parallel to form a battery string in order to achieve a high output voltage and large capacity [4]–[6]. However, manufacturing tolerances result in the differences of the battery capacity and internal resistance from cell to cell [7], [8]. Moreover, these differences will be aggravated with battery aging, leading to the voltage imbalance among cells. When the battery pack is charged or discharged, none of the cells can be overcharged or over-discharged because of the risks of battery performance degradation, even explosion or fire [9]. Therefore, the charging or discharging process has to be interrupted when any of the cells in the battery pack reaches the charging or discharging cut-off voltage, which makes the other cells not being fully charged or discharged and reduces the available capacity of the battery pack [10]. Therefore, battery equalizers are necessary in order to ensure that all cells in a series-connected battery string are fully and safely charged and discharged.

However, the equalizer design for a long battery string is very challenging, which needs to satisfy the high efficiency, ease of control, low voltage stress on MOSFETs, small size, low cost, and easy modularization [11]. Many battery equalizers are proposed during the last few years, which can be classified into two categories: the passive methods and the active ones. The passive balancing method [12] is based on energy dissipation, which employs one dissipative element for each cell as a shunt

to drain excess energy from a high-voltage cell. The advantages of this method are low cost, simple control, and small size. Nevertheless, the excess energy of battery cells is converted into heat rather than be transferred to the low-energy cells, reducing the available capacity of the battery pack. On the other hand, active equalizers present a higher efficiency as they are based on energy transfer. Generally, the active methods are using capacitors [13]–[21], inductors [22]–[26], transformers [27]–[36], or their combination for transferring energy from strong cells (cells with high voltages) to weak ones (cells with low voltages). Among these topologies, transformer-based solutions [27]–[36] have the inherent advantages of easy isolation, high efficiency, and simple implementation. Chen *et al*. [29] propose a bidirectional cell-to-cell equalizer using a multiwinding transformer. The method can transfer energy directly from the source cell to the target one based on flyback or forward conversion, achieving a high balancing speed. However, this equalizer needs two MOSFET switches and one transformer winding for each cell, resulting in a bulk size and high cost of the balancing system. Moreover, the control is very complex due to the requirements of cell voltage sensing circuits and multiple control signals and the judgment of working modes. Hua and Fang [31] propose a charge equalizer based on a modified half-bridge converter, which achieves soft switching and improves the reliability of the equalizer. However, the equalizer needs one winding and two diodes for each cell, as well as one secondary winding and two MOSFET switches for the battery pack. This system still has the disadvantages of high cost and large volume. Moreover, the turns ratio is also extremely high for a long battery string, leading to a low conversion efficiency. In addition, the components in the secondary side of the transformer suffer from high voltage stress, requiring more expensive semiconductor devices. Due to energy transferred from the pack to the least-charged cell, there may be repeated charging and discharging phenomena, resulting in a low balancing efficiency and speed. Lim *et al*. [34] propose a modularized equalizer based on flyback conversion, which does not need cell-voltage-monitoring circuits. The proposed method utilizes the magnetizing energy of the multiwinding transformer for the equalization among modules without the requirement of additional components, leading to a small size and low cost. However, the modularized method is not suitable for more than two battery modules. Zhang *et al*. [35] propose a hierarchical active balancing architecture, which consists of two balancing layers, i.e., the bottom layer and the top layer. The bottom layer employs a buck–boost converter for every two adjacent cells, resulting in a bulk size. Moreover, energy is only transferred from one cell to the adjacent one, leading to a low balancing efficiency and speed. The top layer using a multiwinding transformer is employed to achieve the voltage equalization among battery modules. However, it is definitely difficult to apply one single multiwinding transformer into a long battery string with multiple battery modules because of the high complexity implementation of the multiwinding transformer. Moreover, the mismatched multiple windings cause the natural imbalance of module voltages during the balancing. Li *et al*. [36] propose a simple structure of battery equalizer using multiwinding transformers based on the same EMF induced in different windings. As shown in Fig. 1(a), one MOSFET and one winding of the transformer are set for each cell. Only one control signal is employed for the equalizer, and energy can be automatically and directly delivered from strong cells to weak ones within the battery string [36]. However, this method need additional demagnetizing circuits to reset the magnetic energy stored in the transformer when the MOSFETs are turned off. A suitable capacitor is added for each winding to form a resonant *LC* converter with the magnetizing inductance of the transformer, resulting in the mismatching, high cost, bulk size, and complex design of equalizers. Moreover, this equalizer is only operated in the specific range of switching frequencies and duty cycles to achieve soft switching, leading to more complexity in control and design of the balancing circuits. Although the equalizer only uses one magnetic core and fewer active switches, the implementation is still complicated for a long series-connected battery string due to the mismatching, bulk size, large leakage inductance, and high complexity implementation of the multiple windings.

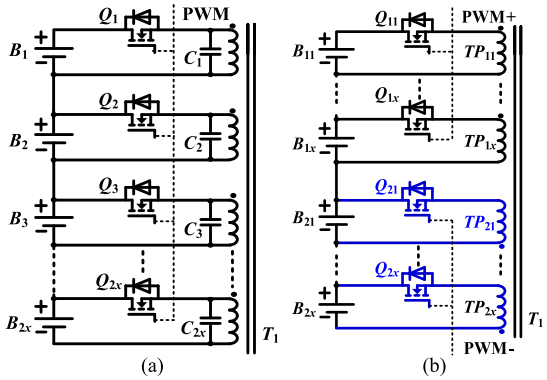

Fig. 1. Battery-balancing circuits using a single multiwinding transformer. (a) The equalizer based on forward conversion [36]. (b) The proposed equalizer based on forward–flyback conversion.

To improve these defects, this paper proposes an automatic equalizer using multiwinding transformer without the needs of additional demagnetizing circuits and cell monitoring circuits. The proposed battery equalizer merges the forward and flyback converters through a common multiwinding transformer. Only one MOSFET and one winding of a transformer are set for each cell. All MOSFETs are controlled by one pair of complementary pulse-width modulation (PWM) signals, and energy can be automatically and directly transferred from any higher voltage cells to any lower voltage cells. Meanwhile, the magnetic energy stored in the transformer is automatically reset due to the complementary structure and control of the proposed equalizer. Moreover, the global equalization among modules can be easily achieved through connecting the secondary sides of multiwinding transformers without the demand of additional components, by which the mismatching problem of multiple windings is solved. The inherent advantages of the proposed system are the small size, low cost, ease of control, high efficiency, fast speed, and easy modularization.

II. Proposed Equalizer

In this paper, an automatic cell equalizer is presented using multiwinding transformers without additional demagnetizing and cell sensing circuits, which is an improvement of the work in [36].

A. Configuration of the Proposed Equalizer

Fig. 1(b) shows the schematic diagram of the proposed equalizer applied to a long battery sting, which is divided into two groups, Group I and Group II, and x cells in each group. Each battery cell is connected by one MOSFET and one primary winding of the multiwinding transformer. As shown in Fig. 1(b), the windings in each group have the same polarities, which are implemented by the conventional forward converter. However, they exhibit opposite polarities compared with these in the other group, which are implemented by the conventional flyback converter. The MOSFETs in the two groups are respectively controlled by one pair of complementary signals, i.e., the MOSFETs in Group I controlled by PWM+, and those in Group II controlled by PWM−.

The critical characteristics of the proposed equalizer are summarized as follows.

1) The proposed equalizer is a hybrid type of forward and flyback converters, which takes full use of the magnetic core, improving the power density.
2) The new combined forward–flyback equalizer needs only one winding and one MOSFET for one cell. Compared with the conventional equalizers using multiwinding transformers, the MOSFET number of the proposed equalizer is reduced by at least half. Moreover, the corresponding floating drive circuits are also reduced greatly. Therefore, the proposed equalizer is smaller and cheaper, and has lower weight.
3) The control for the proposed equalizer is very simple. Only one pair of complementary PWM signals with a fixed frequency and duty ratio are employed to control all MOSFET switches, by which automatic voltage equalization is achieved without the need of cell monitoring circuits.
4) The balancing operation among cells in each group is based on forward conversion, while the balancing operation between the two groups is based on flyback conversion, by which the magnetizing energy stored in the transformers is automatically reset without using additional demagnetizing circuits. This is also beneficial to the size and cost of the equalizer.
5) Due to the effective demagnetization and low turns ratio of the primary windings, low voltage stress on the power devices is achieved, contributing to achievement of high efficiency and low cost.
6) Energy can be transferred automatically, directly, and simultaneously from higher voltage cells at any position to lower voltage cells at any position, i.e., the any-cells-to-any-cells equalization, leading to a high balancing efficiency and speed.

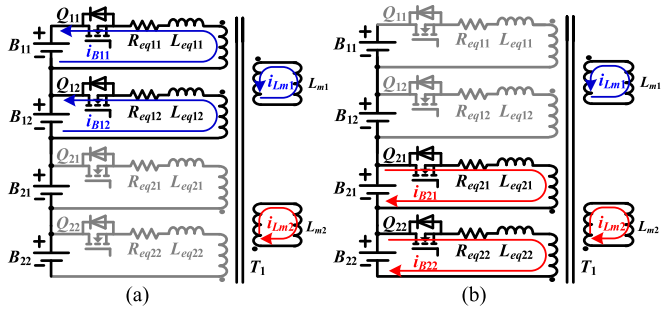

Fig. 2. Operating modes of the proposed equalizer. (a) Mode I. (b) Mode II.

7) The global equalization for a long battery string can be achieved through connecting the secondary sides of multiwinding transformers without using additional components for the equalization among modules. By using this modularization concept, the equalizer design is easier without the mismatching problem of multiple windings.

B. Operation Principles

The automatic balancing among cells can be obtained by driving the MOSFET switches using one pair of complementary PWM signals. The proposed equalizer works on the forward and flyback operations. The forward operation is employed to achieve the voltage equalization among cells in one group. The flyback operation is employed to achieve the voltage equalization between the two groups, and reset the magnetic energy stored in the transformer when some switches are turned off. In order to simplify the analysis for the operation modes, the following assumptions are made.

1) As shown in Fig. 2, the concept is applied to a battery string of four cells, which is modularized into two groups and each group consists of two cells. Fig. 2 shows the equivalent circuit of the proposed equalizer. L_{m1} and L_{m2} represent the magnetizing inductances of Group I and Group II, respectively. $L_{\mathrm{eq}ij}$, $i = 1, 2$, $j = 1, 2$, represents the leakage inductances on a primary winding. $R_{\mathrm{eq}ij}, i = 1, 2, j = 1, 2$, represents the equivalent resistance on a primary winding. Thus, the transformer T_1 can be seen as an ideal transformer.
2) A PWM signal PWM+ is applied to all switches in Group I, and the complementary PWM signal PWM− is applied to all switches in Group II.
3) The relationship among the battery cell voltages is $V_{B22} > V_{B21} > V_{B12} > V_{B11}$.
4) The windings in each group have the same turns number due to the forward operation for each group [36]. N_1 represents the turns number of the primary windings of Group I, and N_2 represents the turns number of the primary windings of Group II.
5) It is specified that the current flowing into a battery cell is positive; otherwise, it is negative.

In the steady state, as shown in Figs. 2 and 3, the proposed equalizer has two operating modes during one switching period, i.e., Mode I and Mode II.

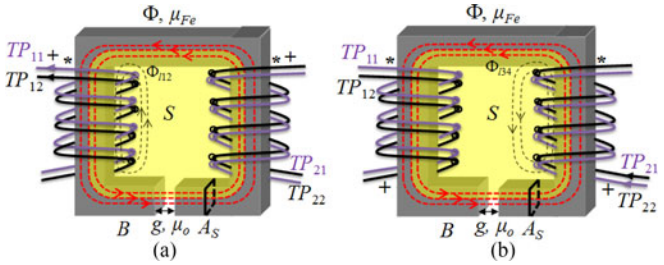

Fig. 3. Magnetic flux analysis. (a) Mode I. (b) Mode II.

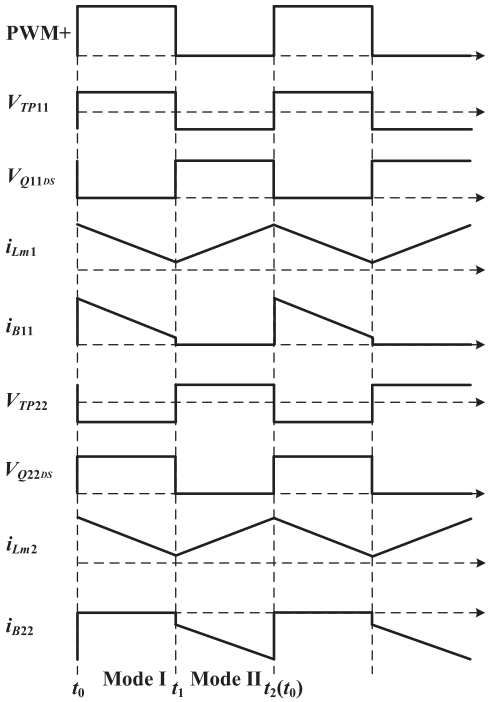

Fig. 4. Key waveforms of the proposed equalizer.

Mode I $(t_0 - t_1)$: At t_0, switches in Group II Q_{21} and Q_{22} are turned off and switches in Group I Q_{11} and Q_{12} are turned on simultaneously.

As shown in Fig. 4, the balancing currents in the primary sides of Group II drop to zero instantaneously at t_0. According to Faraday's law, the balancing currents in the primary sides of Group I are built up to keep the magnetic flux in constant, which resets automatically the magnetization energy in Group II, reducing *dv*/*dt* of MOSFETs Q_{21} and Q_{22}. As shown in Fig. 3(a), the magnetic flux continues to flow counterclockwise, which means the energy stored in the transformer during last mode is transferred to Group I through the flyback converter, achieving the voltage equalization between the two groups.

According to Ampere's law, the magnetic flux can be expressed as

$$\Phi = B \cdot A_S \approx \frac{\mu_0 A_S}{g} N_1 (i_{B11} + i_{B12}) \tag{1}$$

where g is the length of the air gap. B is the flux density. μ_0 is the permeability of the air gap. A_S is the cross-sectional area of the magnetic core. N_1 is the turns number of the primary windings of Group I.

At t_0, the magnetic flux in the transformer is expressed as

$$\begin{aligned}\Phi(t_0) &= \frac{\mu_0 A_S}{g} N_1 \{i_{B11}(t_0) + i_{B12}(t_0)\} \\ &= \frac{\mu_0 A_S}{g} N_2 \{i_{B21}(t_2) + i_{B22}(t_2)\}. \end{aligned} \tag{2}$$

Thus, the initial balancing currents in the primary sides of Group I are achieved by

$$i_{B11}(t_0) + i_{B12}(t_0) = \frac{N_2}{N_1} \{i_{B21}(t_2) + i_{B22}(t_2)\}. \tag{3}$$

The flux linkages of the primary windings of Group I can be expressed as

$$\lambda_{11} = N_1 \Phi = \frac{\mu_0 A_S}{g} {N_1}^2 (i_{B11} + i_{B12}) = L_{m1}(i_{B11} + i_{B12}) \tag{4}$$

$$\lambda_{12} = N_1 \Phi = \frac{\mu_0 A_S}{g} {N_1}^2 (i_{B11} + i_{B12}) = L_{m1}(i_{B11} + i_{B12}) \tag{5}$$

where L_{m1} is given by

$$L_{m1} = \frac{\mu_0 A_S}{g} {N_1}^2. \tag{6}$$

Equation (6) shows the magnetizing inductance is inversely proportional to the air gap.

Based on Faraday's law, the terminal voltages of the primary windings of Group I during Mode I are calculated as

$$\begin{aligned} V_{TP11}(\mathrm{I}) &= \frac{d\lambda_{11}}{dt} = L_{m1}\left(\frac{di_{B11}}{dt} + \frac{di_{B12}}{dt}\right) = \frac{d\lambda_{12}}{dt} \\ &= V_{TP12}(\mathrm{I}). \end{aligned} \tag{7}$$

Equation (7) shows the identical primary voltages will bring the cell voltages to the average value based on forward conversion.

As shown in Fig. 2(a), the charging currents for B_{11} and B_{12} can be represented as

$$i_{B11}(t) = i_{B11}(t_0) - \frac{V_{B11}}{L_{m1} + L_{\mathrm{eq}11}}(t - t_0) \tag{8}$$

$$i_{B12}(t) = i_{B12}(t_0) - \frac{V_{B12}}{L_{m1} + L_{\mathrm{eq}12}}(t - t_0) \tag{9}$$

where V_{B11} and V_{B12} are the cell voltages of B_{11} and B_{12}, respectively. Due to $V_{B12} > V_{B11}$, i_{B12} is smaller than i_{B11}, which also proves the voltage equalization between B_{11} and B_{12} can be achieved by the forward transformer.

The balancing between the two groups is based on flyback conversion. Because the voltage of Group II is higher than the voltage of Group I, energy is transferred from Group II to Group I. The relationship between the primary voltages of the two groups is determined by [37]–[39]

$$\frac{V_{TP2}(II)}{V_{TP1}(I)} = \frac{N_2}{N_1}\frac{D}{1 - D} \tag{10}$$

where D is the duty cycle for Group I. $V_{TP1}(I)$ represents the uniform primary voltage of Group I during Mode I. $V_{TP2}(\mathrm{II})$ represents the uniform primary voltage of Group II during Mode II. $V_{TP1}(I)$ and $V_{TP2}(\mathrm{II})$ can be given by

$$V_{TP1}(\mathrm{I}) = V_{TP11}(\mathrm{I}) = V_{TP12}(\mathrm{I})$$
$$V_{TP2}(\mathrm{II}) = V_{TP21}(\mathrm{II}) = V_{TP22}(\mathrm{II}). \quad (11)$$

Equation (10) can be deduced as

$$D = \frac{N_1 V_{TP2}(\mathrm{II})}{N_1 V_{TP2}(\mathrm{II}) + N_2 V_{TP1}(\mathrm{I})}. \quad (12)$$

In order to achieve the voltage equalization for the battery string, the primary voltages of Group I and Group II should satisfy

$$V_{TP1}(\mathrm{I}) = V_{TP2}(\mathrm{II}) = V_{\mathrm{avg}} \quad (13)$$

where V_{avg} is the average voltage of the battery string.

By (12) and (13), the duty cycle D can be obtained as

$$D = \frac{N_1}{N_1 + N_2}. \quad (14)$$

The magnetizing currents i_{Lm1} and i_{Lm2} are expressed as

$$i_{Lm1}(t) = i_{Lm1}(t_0) - \frac{V_{\mathrm{avg}}}{L_{m1}}(t - t_0) \quad (15)$$

$$i_{Lm2}(t) = i_{Lm2}(t_0) - \frac{N_2 V_{\mathrm{avg}}}{N_1 L_{m2}}(t - t_0). \quad (16)$$

The relationship among the magnetizing currents and the balancing currents in the primary windings of Group I can be expressed as follows:

$$i_{Lm1} + \frac{N_2}{N_1} i_{Lm2} = i_{B11} + i_{B12}. \quad (17)$$

The main function of this mode is to balance the cell voltages of Group I, deliver the energy stored in the magnetizing inductors L_{m1} and L_{m2} to Group I, and achieve the demagnetization of the second group when the switches Q_{21} and Q_{22} are turned off.

Mode II $(t_1 - t_2)$: At t_1, switches in Group I Q_{11} and Q_{12} are turned off and switches in Group II Q_{21} and Q_{22} are turned on simultaneously.

As shown in Fig. 4, the balancing currents in the primary sides of Group I drop to zero instantaneously at t_1. According to Faraday's law, the balancing currents in the primary sides of Group II are built up to keep the magnetic flux in constant, which resets automatically the magnetizing energy stored in Group I, reducing *dv/dt* of MOSFETs Q_{11} and Q_{12}. As shown in Fig. 3(b), the magnetic flux flows counterclockwise, which means the energy of Group II is stored in the transformer.

The mathematical derivation of Mode II is similar to Model I, thereby not described in detail here.

The initial currents in the primary sides of Group II can be expressed as

$$i_{B21}(t_1) + i_{B22}(t_1) = \frac{N_1}{N_2}\left\{i_{B11}(t_1) + i_{B12}(t_1)\right\}. \quad (18)$$

The terminal voltages of the primary windings of Group II during Mode II are calculated as

$$V_{TP21}(\mathrm{II}) = \frac{d\lambda_{21}}{dt} = L_{m2}\left(\frac{di_{B21}}{dt} + \frac{di_{B22}}{dt}\right) = \frac{d\lambda_{22}}{dt}$$
$$= V_{TP22}(\mathrm{II}). \quad (19)$$

The discharging currents from B_{21} and B_{22} are given by

$$i_{B21}(t) = i_{B21}(t_1) - \frac{V_{B21}}{L_{m2} + L_{\mathrm{eq21}}}(t - t_1) \quad (20)$$

$$i_{B22}(t) = i_{B22}(t_1) - \frac{V_{B22}}{L_{m2} + L_{\mathrm{eq22}}}(t - t_1) \quad (21)$$

where V_{B22} and V_{B22} are the cell voltages of B_{21} and B_{22}, respectively. Due to $V_{B22} > V_{B22}$, i_{B21} is smaller than i_{B22}, which also proves the voltage equalization between B_{21} and B_{22} is achieved through the forward transformer.

The magnetizing currents i_{Lm1} and i_{Lm2} are expressed as

$$i_{Lm1}(t) = i_{Lm1}(t_1) + \frac{N_1 V_{\mathrm{avg}}}{N_2 L_{m1}}(t - t_1) \quad (22)$$

$$i_{Lm2}(t) = i_{Lm2}(t_1) + \frac{V_{\mathrm{avg}}}{L_{m2}}(t - t_1). \quad (23)$$

The relationship among the magnetizing currents and the balancing currents in Group II can be represented as

$$-i_{B21} - i_{B22} = \frac{N_1}{N_2} i_{Lm1} + i_{Lm2}. \quad (24)$$

The main function of this mode is to balance the cell voltages in Group II, deliver energy of the cells in Group II into the magnetizing inductors L_{m1} and L_{m2}, and achieve the demagnetization of the first group when the switches Q_{11} and Q_{12} are turned off.

According to the operating modes mentioned earlier, the magnetizing currents i_{Lm1} and i_{Lm2} can flow naturally between the two groups without the requirement of additional demagnetizing circuits, by which the effective balancing among all cells is achieved.

C. Modularization of the Proposed Equalizer

Fig. 5 shows the modularization method of the proposed equalizers applied to an eight-cell series-connected battery string, which is divided into two separate four-cell modules. The equalization between modules is easily achieved through connecting the secondary sides of the two transformers. Contrary to the conventional modularized equalizers using additional components for the equalization among modules, the proposed modularization method shares a single equalizer for the equalization among cells and modules, leading to smaller size, lower cost, and reduced loss with respect to the modularization. This modularization method also overcomes the mismatching problem of multiple windings.

TABLE I
COMPARISON OF SEVERAL BATTERY EQUALIZERS

Balancing performance	Components						P_1	P_2	P_3	P_4	P_5	P_6	P_7	P_8	P_9	P_{10}	P_{11}	P_{12}	P_{avg}
	SW	R	L	C	D	T													
Dissipative method [12]	n	n	0	0	0	0	5	1	1	1	1	5	1	5	5	3	5	1	2.83
Switched capacitors [13]	$2n$	0	0	$n-1$	0	0	5	3	5	5	1	2	4	5	5	3	5	4	3.92
Chain structure of switched capacitors [15]	$2(n+2m)$	0	0	$n+m$	0	0	4	4	5	5	2	3	3	4	4	2	5	4	3.75
ZCS switched capacitors [18]	$2n$	0	$n-1$	$n-1$	0	0	3	3	5	5	1	3	3	4	3	3	5	5	3.58
LC series resonant circuit [19]	$2(n+5m)$	0	m	m	0	0	3	4	2	5	2	2	3	2	3	2	1	5	2.83
Buck–boost converter [22]	$2n$	0	$n-1$	0	0	0	4	3	5	5	2	2	3	3	3	5	5	2	3.50
Multiphase interleaved method [23]	$2(n-1)$	0	$n-1$	0	0	0	4	4	5	5	4	4	3	4	3	2	3	2	3.58
Optimized next-to-next balancing [24]	$4(n-1)$	0	$2(n-1)$	0	0	0	3	3	5	5	2	2	2	4	2	4	5	1	3.17
Flyback or forward conversion [29]	$2n$	0	0	0	0	m	2	3	5	5	3	3	3	2	3	3	5	3	3.33
Flyback conversion [32]	$2(n-m)$	0	0	0	$2(n-m)$	m	3	4	2	1	3	3	2	2	3	3	2	2	2.50
Wave-trap [33]	$2m$	0	n	n	n	n	2	3	1	1	3	3	1	1	2	1	1	5	2.00
Forward conversion [36]	n	0	0	n	0	m	3	5	5	5	5	5	5	3	4	5	4	5	4.50
Proposed equalizer	n	0	0	0	0	m	4	4	5	5	5	5	5	5	5	5	5	4	4.75

n is the number of cells in the battery string. m is the number of battery modules in the battery string.

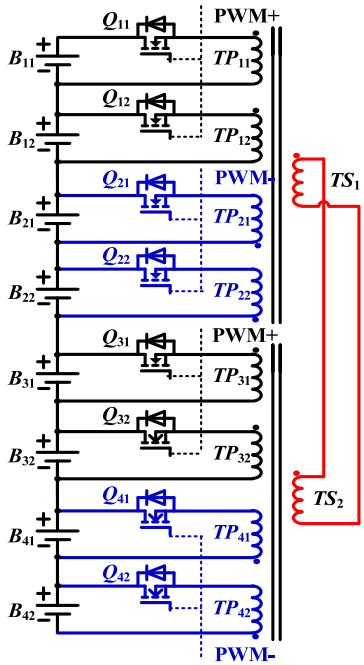

Fig. 5. Modularized structures of the proposed equalizer for a battery string of eight cells, which are divided into two modules.

D. Comparison with Conventional Battery Equalizers

In order to systematically evaluate the proposed scheme, Table I gives a comparative study with conventional battery equalizers focusing on the components and the balancing performances. "Components" mainly focuses on the numbers of switches (SW), resistors (R), inductors (L), capacitors (C), diodes (D), and transformers (T). In addition, 12 parameters are employed to evaluate the balancing performances. Each parameter is fuzzified into five fuzzy scales, for which "1," "2," "3," "4," and "5" represent the worst, bad, neutral, good, and best performances, respectively. The balancing performance parameters consist of cost (P_1), efficiency (P_2), whether automatic balancing (P_3), whether bidirectional balancing (P_4), energy flow (P_5), speed (P_6), implementation feasibility (P_7), control simplicity (P_8), size (P_9), modularity (P_{10}), switch voltage stress (P_{11}), and switch current stress (P_{12}). The balancing efficiency is evaluated according to the average energy conversion efficiency for one switching step and the average switching steps to transfer energy from the source cell to the target one. The energy flow is evaluated according to the balancing paths, e.g., 1: adjacent cell-to-cell, 2: direct cell-to-cell, 3: pack-to-cell or cell-to-pack, 4: cell-to-pack-to-cell, and 5: any-cells-to-any-cells. The equalization speed is determined by the equalization power, the number of cells involved in balancing at the same time, and the average switching steps to complete the charge transportation from the source cell to the target one. Implementation feasibility is evaluated according to the practical application possibility of the equalizer for a long series-connected battery string in electric vehicles. Control simplicity is evaluated according to the number of the control signal, the complexity of the control signal generation, and the necessity of cell voltage monitoring. Modularity is evaluated according to the number of elements for the equalization among modules and the expandability. A comparison can be carried out based on the average score P_{avg}. It can be observed that the proposed equalizer has the highest score, and has the advantages of low cost, small size, high efficiency, high speed, low voltage stress, and easy modularization, due to which the proposed topology has very good implementation possibility to be applied to a long series-connected battery string. In Table I, the average score is calculated based on the same weight for each parameter. In fact, the parameter weight should be modified according to different practical applications.

In order to further verify the advantages of the proposed equalizer, Table II presents a quantified comparison between the proposed equalizer and the forward one [36]. Due to all cells connected to the same magnetic core, the balancing power of the two methods is mainly determined by the voltage difference among cells. Thus, they have the same balancing power rating. These two solutions can transfer energy directly and simultaneously from any higher voltage cells to any lower voltage cells.

TABLE II
COMPARISON OF THE PROPOSED EQUALIZER WITH THE FORWARD SOLUTION [36]

Equalizers	Number of MOSFETs	Number of Windings	Operation Principles	Demagnetizing Circuits		Balancing Speed ($\mathrm{Step}_{\mathrm{avg}}$)	Balancing Efficiency	Size	Cost
Forward equalizer [36]	n	n	Forward conversion	Need	1	Simultaneous balancing	η_{fw}	Large	High
Proposed equalizer	n	n	Forward and flyback conversion	No need	1	Simultaneous balancing	$\frac{\eta_{fw}+\eta_{fy}}{2}$	Small	Low

Note: η_{fw} is the efficiency of the forward conversion. η_{fy} is the efficiency of the flyback conversion.

Theoretically, it only takes one balancing step for these two methods to complete the charge transportation from the source cells to the target ones without intermediate steps. Moreover, the balancing speed is independent of the number of battery cells and the initial cell voltages. Therefore, the proposed equalizer has the same balancing speed compared with the forward equalizer [36]. Due to the direct and simultaneous any-cells-to-any-cells equalization, the balancing efficiency is mainly determined by the average energy conversion efficiency. The equalizer in [36] is based on forward conversion, while the proposed solution is based on forward–flyback conversion. The forward converter transfers energy instantly across the transformer and does not rely on energy storage in the transformer, while the flyback converter stores energy in the magnetic field before transferring to the output of the converter. Therefore, the forward converter is generally more energy efficient than the flyback one. In addition, in [36], as shown in Fig. 1(a), the energy of magnetizing reset is regenerated into the capacitors connected in parallel with the windings. In contrast, in the proposed method, the regenerative energy can be routed to the lower voltage group automatically, thereby achieving an effective cell equalization. Nevertheless, the equalizer in [36] achieves soft switching, which is beneficial to the improvement of the equalization efficiency. Overall, the balancing efficiency of the proposed equalizer is slightly lower than that in [36]. In fact, the proposed equalizer has the advantages of smaller size, lower cost, and easier control due to the absence of demagnetizing circuits.

III. EXPERIMENTAL RESULTS

To show the feasibility of the proposed equalizer, a prototype for four lithium-ion cells connected in series was implemented. Fig. 6 shows a photograph of the experimental setup. STP220N6F7 MOSFETs with 2.4-mΩ drain–source on-resistance were used for all MOSFET switches. dSPACE was used for the digital control, which can generate a pair of complementary PWM singles to control the MOSFETs in the two battery groups, and receive the cell voltage information by analog-to-digital converters. Eight 2600-mAh $LiNiMnCoO_2$ battery cells and eight 1100-mAh $LiFePO_4$ battery cells were used during experiments. The parameters of the multiwinding transformers are summarized in Table III.

A. Consideration for Transformers

The key design parameters of the transformer consist of the duty cycle D, turns ratio N, switch frequency f, magnetizing inductance L_m, and air gap g.

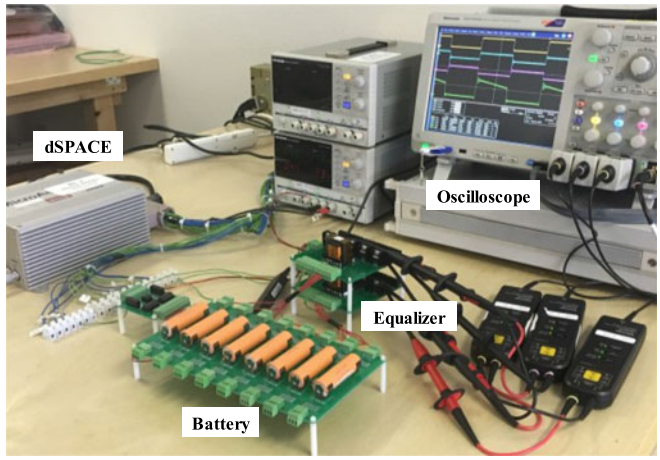

Fig. 6. Experimental setup.

1) Duty Cycle D: It is assumed that the input voltage $V_{\mathrm{in\,max}}$ is 4.2 V in the extreme condition, the output voltage $V_{\mathrm{o\,min}}$ is 3 V in the extreme condition, the peak equalizing current $i_{\mathrm{peak}} \leq 1$ A, and the switching frequency is set for 15 kHz.

To prevent a reverse current flow from the weak cell to the transformer, the flyback converter should be operated in continuous current mode, then

$$\begin{cases} DT\dfrac{V_{\mathrm{in\,max}}}{L_m+L_{\mathrm{eq}}} - (1-D)T\dfrac{V_{o\,\mathrm{min}}}{L_m+L_{\mathrm{eq}}} \geq 0 \\ (1-D)T\dfrac{V_{\mathrm{in\,max}}}{L_m+L_{\mathrm{eq}}} - DT\dfrac{V_{o\,\mathrm{min}}}{L_m+L_{\mathrm{eq}}} \geq 0 \end{cases} \tag{25}$$

where T is the switching period.

By solving (25), the duty cycle D can be derived as

$$41.7\% \leq D \leq 58.3\%. \tag{26}$$

Due to the complementary structure of the transformer, the desired duty cycle is 50%.

2) Turns Ratio N: According to (14), with $D = 50\%$, the turns ratio is calculated as

$$N = N_1 : N_2 = 1 : 1. \tag{27}$$

3) Magnetizing Inductance L_m: To make full use of the energy of the transformer and prevent the core saturation, the peak discharging current during any mode was limited to −1 A. Moreover, it is assumed that the initial discharge current in each switching cycle i_0 is −0.1 A. According to (23), the magnetizing inductance of the multiwinding transformer can be

TABLE III
PARAMETERS OF THE MULTIWINDING TRANSFORMERS

	Transformer I					Transformer II				
	TP_{11}	TP_{12}	TP_{21}	TP_{22}	TS_1	TP_{31}	TP_{32}	TP_{41}	TP_{42}	TS_2
L_m (μH)	158.1	157.6	157.7	157.5	2460	157.2	157.3	157.1	157.2	2480
L_{eq} (μH)	0.24	0.23	0.22	0.21	36.7	0.29	0.28	0.34	0.34	39.6
R_{eq} (Ω)	0.52	0.51	0.52	0.51	7.53	0.51	0.51	0.51	0.52	7.82
N_P			17.5					17.5		
N_S			69.5					69.5		

Note: N_P is the turn number of the primary windings. N_S is the turn number of the secondary winding.

obtained as follows:

$$L_m \geq \frac{V_{\text{in max}}}{|i_{\text{peak}} - i_0|} DT = 155.6\,\mu\text{H}. \tag{28}$$

In fact, a large magnetizing inductance will weaken the effect of flyback conversion and enhance the effect of forward conversion, resulting in a reduction in the balancing performance. Thus, the magnetizing inductance is set as the marginal value of 155.6 μH.

4) Air Gap g: The proposed equalizer merges the flyback and forward converters through a common transformer. The forward converter does not rely on energy storage, thereby, does not need air gap in the transformer. Nevertheless, the flyback converter stores energy in the transformer before transferring to the output of the converter, which needs air gap. Therefore, air gap should be carefully designed while considering the trade-off between the forward conversion and flyback conversion. According to (6) and (28), a reasonable air gap can be achieved by

$$g \leq N_1 \frac{\mu_0 A_S}{L_m}. \tag{29}$$

B. Experimental Waveforms and Balancing Efficiencies

Fig. 7 shows the experimental waveforms for Group I and Group II at $f = 15$ kHz. All of the switches in Group I are driven by PWM+, and all of the switches in Group II are driven by the complementary signal PWM-. Since the voltage of Group II is higher than the voltage of Group I, energy is automatically transferred from Group II to Group I. Fig. 7(a) shows the experimental waveforms for Group I. It can be seen that when the MOSFETs Q_{11}–Q_{12} are turned on, i_{B11} flows from the multiwinding transformer to B_{11}. Due to the magnetic energy stored in the multiwinding transformer during the last mode, i_{B11} increases rapidly and then decreases linearly. The root-mean-square (RMS) balancing current regenerated to B_{11} is approximately 370.1 mA. When the MOSFET switch Q_{11} is turned off, the maximum voltage stress on Q_{11} does not exceed 8 V, even in the voltage spikes, greatly reducing *dv*/*dt* of the MOSFETs. This shows that the effective demagnetization for Group I is achieved when switches Q_{11}–Q_{12} are turned off. These results agree well with the theoretical waveforms shown in Fig. 4.

Fig. 7(b) shows the experimental waveforms for Group II at $f = 15$ kHz. When the MOSFETs Q_{21}–Q_{22} are turned on, i_{B22} flows from the battery cell B_{22} to the multiwinding transformer. During this mode, energy is stored into the multiwinding transformer from the battery cells. The RMS balancing current flowing out of B_{22} is approximately 343.7 mA. When the MOSFET switch Q_{22} is turned off, the maximum voltage stress on Q_{22} does not exceed 8 V, greatly reducing *dv*/*dt* of the MOSFETs. This shows that the proposed complementary structure

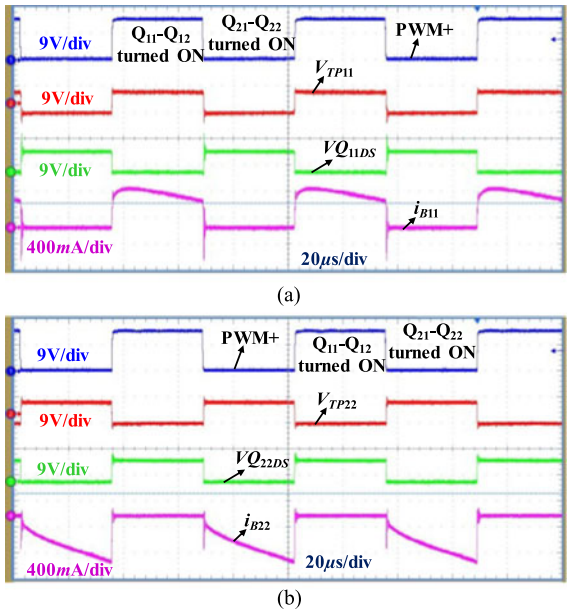

Fig. 7. Experimental waveforms of the primary voltages, balancing currents, and switch voltage stress at the frequency of $f = 15$ kHz. (a) Group I. (b) Group II.

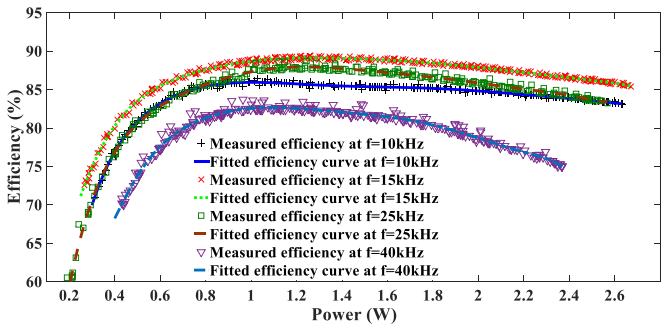

Fig. 8. Measured balancing efficiency η_e as a function of power at different frequencies.

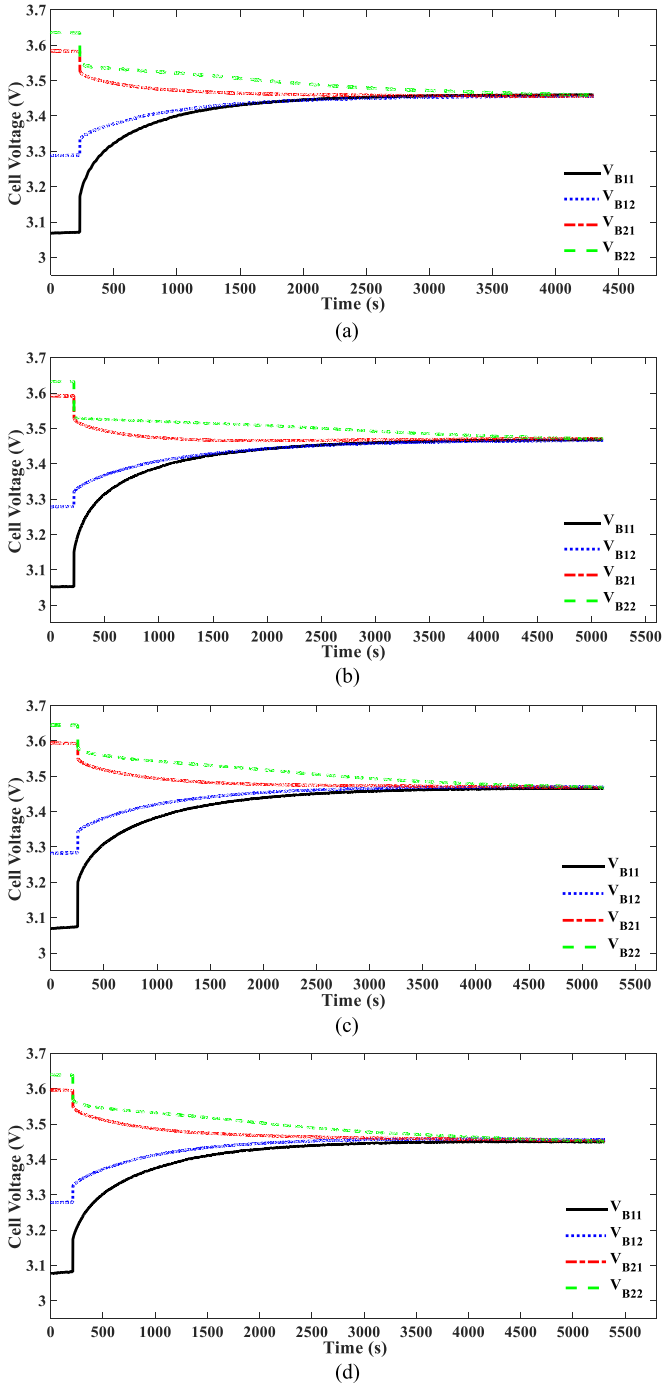

Fig. 9. Experimental results for four $LiNiMnCoO_2$ cells at different frequencies. (a) $f = 10$ kHz. (b) $f = 15$ kHz. (c) $f = 25$ kHz. (d) $f = 40$ kHz.

achieves the effective demagnetization for Group II when the switches $Q_{11}-Q_{12}$ are turned off.

Fig. 8 shows the measured efficiency η_e as a function of power at different frequencies. At the frequency of $f = 10$ kHz, when the input power increases from 0.31 W to 0.96 W, η_e increases from 71% to the maximum of 85.8%. However, when the input power continues to increase to 2.63 W, η_e decreases from 85.8% to 83.1%. At $f = 15$ kHz, η_e reaches up to the maximum of 89.4% at the power of 1.26 W, and then decreases to 85.6% at the power of 2.66 W. At $f = 25$ kHz, η_e reaches up to the maximum of 88.6% when the input power is 1.12 W. At $f = 40$ kHz, the highest efficiency of 82.7% is achieved at the input power of 1.10 W. These results show that the proposed equalizer can work with a high efficiency at different frequencies, and achieves the highest efficiency of 89.4% at $f = 15$ kHz.

TABLE IV
BALANCING RESULTS AT DIFFERENT FREQUENCIES

Frequency (kHz)	$f = 10$	$f = 15$	$f = 25$	$f = 40$
Balancing time (s)	4300	5100	5200	5300
Balanced voltage (V)	3.460	3.469	3.465	3.455
Voltage gap before balancing (mV)	566	581	573	559
Voltage gap after balancing (mV)	5	5	4	6

C. Cell-Balancing Results

Fig. 9 shows the experimental results for four $LiNiMnCoO_2$ cells at different frequencies. The initial cell voltages are 3.052, 3.279, 3.592, and 3.637 V, respectively. B_{11} has the lowest voltage, B_{22} has the highest voltage among the four cells, and the initial maximum voltage gap is 0.585 V. Table IV summarizes the balancing results in terms of the balancing time, balanced voltage, and voltage gap before and after balancing. It is important to note that the higher balanced cell voltage represents the higher equalization efficiency. It can be observed that the equalization at the frequency of 15 kHz has the highest efficiency, which agrees well with the measured efficiency results shown in Fig. 8. The fastest balancing is achieved at the frequency of 10 kHz. The best equalization with 4-mV voltage gap among cells is achieved at the frequency of 25 kHz. It can be concluded that the proposed equalizer can work at a wide range of frequencies.

Fig. 10 shows the equalization results with different initial voltages compared with Fig. 9. It can be observed that the equalization for the two imbalanced situations is well executed by the proposed equalizer. This proves that the proposed balancing operation is independent of the cell initial voltages and positions in the series-connected battery string, showing the good robustness of the proposed equalizer.

In order to prove the validity of the proposed scheme in terms of the dynamic equalization, Fig. 11 shows the balancing results during the constant current charging and discharging of the battery pack. As shown in Fig. 11(a), all the cells are almost identically charged with the proposed equalization method, and the maximum voltage difference is reduced greatly from 492 mV to 8 mV. As shown in Fig. 11(b), a similar situation occurs when the battery pack is discharged. It can be observed that the consistency and the available capacity of the battery pack during charging and discharging are greatly improved by the proposed equalization scheme.

Fig. 12 shows the experimental results for $LiFePO_4$ batteries with unequal cell numbers in different groups at $f = 15$ kHz. As shown in Fig. 12(a)–(d), the voltage equalization is well ex-

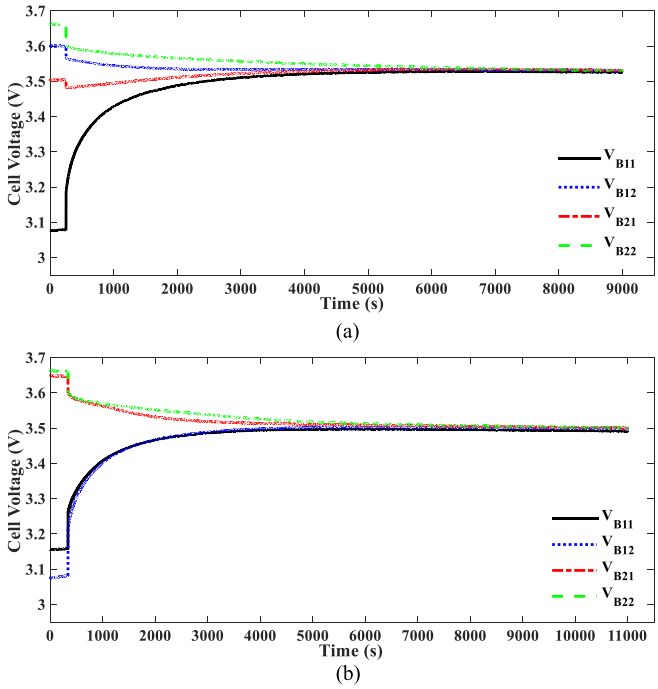

Fig. 10. Experimental results for four $LiNiMnCoO_2$ cells with different initial voltages at $f = 15$ kHz.

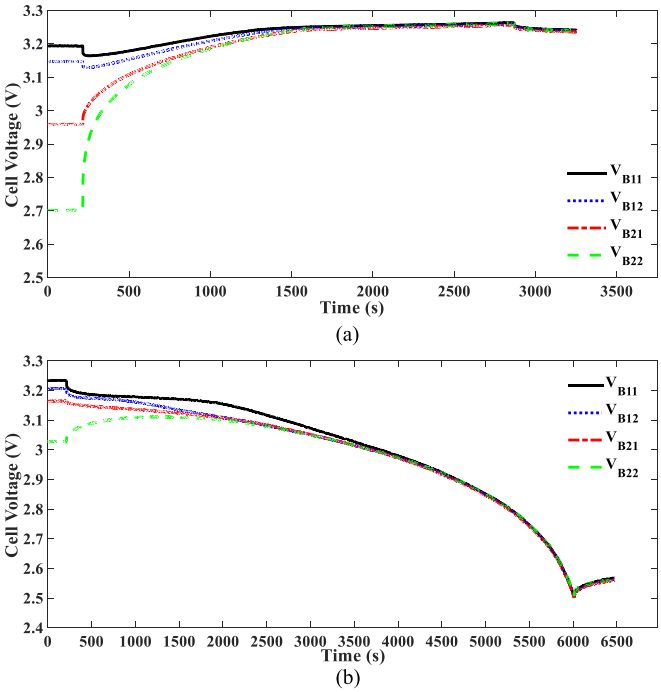

Fig. 11. Dynamic balancing results for four $LiFePO_4$ cells. (a) Battery charge. (b) Battery discharge.

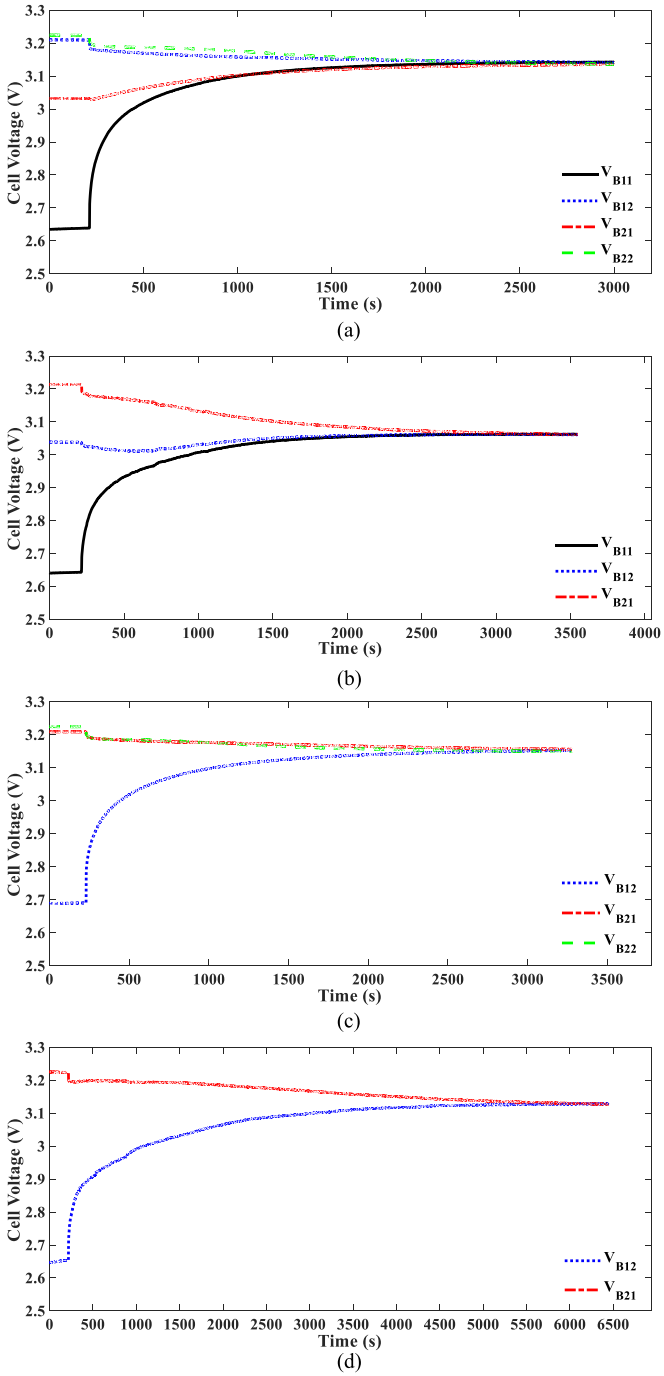

Fig. 12. Experimental results for $LiFePO_4$ cells with unequal cell numbers in different groups at $f = 15$ kHz. (a) Two cells in Group I and two cells Group II. (b) Two cells in Group I and one cell in Group II. (c) One cell in Group I and two cells in Group II. (d) One cell in Group I and One cell in Group II.

ecuted by the proposed equalizer even though there are unequal numbers of cells in the two groups. It can be concluded that the balancing performance is not affected by the unequal cell numbers in different groups and the combining forms of forward and flyback converters, which demonstrates that the proposed equalizer is easy to modulate and has no limit on the numbers of battery cells in different groups.

Fig. 13 shows the modularized equalization result for eight $LiNiMnCoO_2$ cells at $f = 15$ kHz. The initial cell voltages are 3.566, 3.530, 3.216, 3.022, 3.647, 3.635, 3.421, and 3.311 V, respectively. The initial maximum voltage gap among cells is 0.625 V. After about 6900 s, a balanced voltage of 3.463 V is

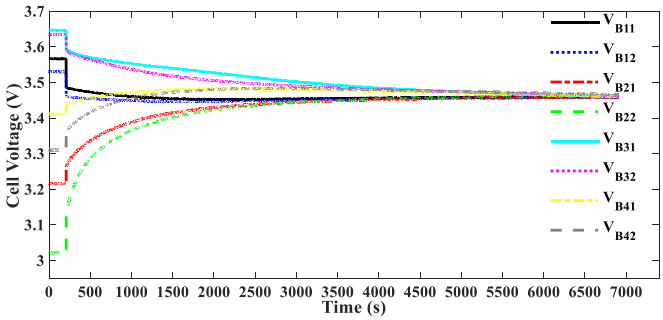

Fig. 13. Modularized equalization result for eight $LiNiMnCoO_2$ cells, which are divided into two separate four-cell modules at $f = 15$ kHz.

achieved, and the voltage gap among cells is 9 mV. This verifies the validity of the proposed modularized equalizer.

IV. Conclusion

An automatic any-cells-to-any-cells battery equalizer using multiwinding transformers is proposed based on forward–flyback conversion, and a prototype for four cells is implemented. The configuration of the proposed equalizer, the operation principles, the modular design, the comparative studies, and the cell balancing results are presented in this paper. The practical implementation presented in this paper has shown that the proposed equalizer achieves efficient voltage equalization regardless of the battery working state (rest, charging, or discharging) without the needs of cell monitoring and additional demagnetizing circuits. Moreover, the proposed topology has a high balancing efficiency of 89.4% and obtains a low voltage stress on all MOSFET switches, thereby ensuring the equalization scheme high reliability. In addition, this method is easily modularized and is not limited to the numbers of the battery cells in modules. Since this topology requires a minimum number of passive components and has outstanding balancing performances, it promises to solve the dilemmas of battery equalizers applied to a long series-connected battery string to be used in electric vehicles.

References

[1] J. Jiang, Q. Liu, C. Zhang, and W. Zhang, "Evaluation of acceptable charging current of power li-ion batteries based on polarization characteristics," *IEEE Trans. Ind. Electron.*, vol. 61, no. 12, pp. 6844–6851, Dec. 2014.

[2] M. Gholizadeh and F. R. Salmasi, "Estimation of state of charge, unknown nonlinearities, state of health of a lithium-ion battery based on a comprehensive unobservable model," *IEEE Trans. Ind. Electron.*, vol. 61, no. 3, pp. 1335–1344, Mar. 2014.

[3] C. Zhang, L. Y. Wang, X. Li, W. Chen, G. G. Yin, and J. Jiang, "Robust and adaptive estimation of state of charge for lithium-ion batteries," *IEEE Trans. Ind. Electron.*, vol. 62, no. 8, pp. 4948–4957, Aug. 2015.

[4] B. Xia and C. Mi, "A fault-tolerant voltage measurement method for series connected battery packs," *J. Power Sources*, vol. 308, pp. 83–96, Mar. 2016.

[5] B. Xia, Y. Shang, T. Nguyen, and C. Mi, "A correlation based fault detection method for short circuits in battery packs," *J. Power Sources*, vol. 337, pp. 1–10, Jan. 2017.

[6] E. Chatzinikolaou and D. J. Rogers, "Cell SoC balancing using a cascaded full-bridge multilevel converter in battery energy storage systems," *IEEE Trans. Ind. Electron.*, vol. 63, no. 9, pp. 5394–5402, Sep. 2016.

[7] J. Chatzakis, K. Kalaitzakis, N. C. Voulgaris, and S. N. Manias, "Designing a new generalized battery management system," *IEEE Trans. Ind. Electron.*, vol. 50, no. 5, pp. 990–999, Oct. 2013.

[8] W. Huang and J. A. Qahouq, "Energy sharing control scheme for state-of-charge balancing of distributed battery energy storage system," *IEEE Trans. Ind. Electron.*, vol. 62, no. 5, pp. 2764–2776, May 2015.

[9] K.-M. Lee, S.-W. Lee, Y.-G. Choi, and B. Kang, "Active balancing of li-ion battery cells using transformer as energy carrier," *IEEE Trans. Ind. Electron.*, vol. 64, no. 2, pp. 1251–1257, Feb. 2017.

[10] C.-M. Young, N.-Y. Chu, L.-R. Chen, Y.-C. Hsiao, and C.-Z. Li, "A single-phase multilevel inverter with battery balancing," *IEEE Trans. Ind. Electron.*, vol. 60, no. 5, pp. 1972–1978, May 2013.

[11] J. G. Lozano and E. R. Cadaval, "Battery equalization active methods," *J. Power Sources*, vol. 246, pp. 934–949, 2014.

[12] G.-L. Javier, R.-C. Enrique, M. I. Milanes-Montero, and M. A. Guerrero-Martinez, "A novel active battery equalization control with on-line unhealthy cell detection and cell change decision," *J. Power Sources*, vol. 299, pp. 356–370, 2015.

[13] C. Pascual and P. T. Krein, "Switched capacitor system for automatic series battery equalization," in *Proc. IEEE Appl. Power Electron. Conf.*, 1997, pp. 848–854.

[14] A. C. Baughman and M. Ferdowsi, "Double-tiered switched-capacitor battery charge equalization technique," *IEEE Trans. Ind. Electron.*, vol. 55, no. 6, pp. 2277–2285, Jun. 2008.

[15] M.-Y. Kim, C.-H. Kim, J.-H. Kim, and G.-W. Moon, "A chain structure of switched capacitor for improve cell balancing speed of lithium-ion batteries," *IEEE Trans. Ind. Electron.*, vol. 61, no. 8, pp. 3989–3999, Aug. 2014.

[16] Y. Shang, B. Xia, F. Lu, C. Zhang, N. Cui, and C. Mi, "A switched-coupling-capacitor equalizer for series-connected battery strings," *IEEE Trans. Power Electron.*, to be published, doi:10.1109/TPEL.2016.2638318.

[17] M. Uno and K. Tanaka, "Single-switch multioutput charger using voltage multiplier for series-connected lithium-ion battery/supercapacitor equalization," *IEEE Trans. Ind. Electron.*, vol. 60, no. 8, pp. 3227–3239, Aug. 2013.

[18] Y. Ye, K. W. E. Cheng, and Y. P. B. Yeung, "Zero-current switching switched-capacitor zero-voltage-gap automatic equalization system for series battery string," *IEEE Trans. Power Electron.*, vol. 27, no. 7, pp. 3234–3242, Jul. 2012.

[19] K. Lee, Y. Chung, C.-H. Sung, and B. Kang, "Active cell balancing of li-ion batteries using LC series resonant circuit," *IEEE Trans. Ind. Electron.*, vol. 62, no. 9, pp. 5491–5501, Sep. 2015.

[20] Y. Shang, C. Zhang, N. Cui, and J. M. Guerrero, "A cell-to-cell battery equalizer with zero-current switching and zero-voltage gap based on quasi-resonant LC converter and boost converter," *IEEE Trans. Power Electron.*, vol. 30, no. 7, pp. 3731–3747, Jul. 2015.

[21] Y. Shang, C. Zhang, N. Cui, K. Sun, and J. M. Guerrero, "A crossed pack-to-cell equalizer based on quasi-resonant LC converter with adaptive fuzzy logic equalization control for series-connected lithium-ion battery strings," in *Proc. IEEE Appl. Power Electron. Conf.*, 2015, pp. 1685–1692.

[22] M.-Y. Kim, J.-H. Kim, and G.-W. Moon, "Center-cell concentration structure of a cell-to-cell balancing circuit with a reduced number of switches," *IEEE Trans. Power Electron.*, vol. 29, no. 10, pp. 5285–5297, Oct. 2014.

[23] F. Mestrallet, L. Kerachev, J.-C. Crebier, and A. Collet, "Multiphase interleaved converter for lithium battery active balancing," *IEEE Trans. Power Electron.*, vol. 29, no. 6, pp. 2874–2881, Jun. 2014.

[24] T. H. Phung, A. Collet, and J.-C. Crebier, "An optimized topology for next-to-next balancing of series-connected lithium-ion cells," *IEEE Trans. Power Electron.*, vol. 29, no. 9, pp. 4603–4613, Sep. 2014.

[25] P. A. Cassani and S. S. Williamson, "Design, testing, and validation of a simplified control scheme for a novel plug-in hybrid electric vehicle battery cell equalizer," *IEEE Trans. Ind. Electron.*, vol. 57, no. 12, pp. 3956–3962, Dec. 2010.

[26] Y.-S. Lee and M.-W. Cheng, "Intelligent control battery equalization for series connected lithium-ion battery strings," *IEEE Trans. Ind. Electron.*, vol. 52, no. 5, pp. 1297–1307, Oct. 2005.

[27] L. McCurlie, M. Preindl, and A. Emadi, "Fast model predictive control for redistributive lithium ion battery balancing," *IEEE Trans. Ind. Electron.*, vol. 64, no. 2, pp. 1350–1357, Feb. 2017.

[28] M. Uno and A. Kukita, "Double-switch equalizer using parallel-or series–parallel-resonant inverter and voltage multiplier for series-connected supercapacitors," *IEEE Trans. Power Electron.*, vol. 29, no. 2, pp. 812–828, Feb. 2014.

[29] Y. Chen, X. Liu, Y. Cui, J. Zou, and S. Yang, "A multi-winding transformer cell-to-cell active equalization method for lithium-ion batteries with reduced number of driving circuits," *IEEE Trans. Power Electron.*, vol. 31, no. 7, pp. 4916–4929, Jul. 2016.
[30] A. Tasuku and H. Koizumi, "Double-input bidirectional DC/DC converter using cell-voltage equalizer with flyback transformer," *IEEE Trans. Power Electron.*, vol. 30, no. 6, pp. 2923–2934, Jun. 2015.
[31] C. Hua and Y.-H. Fang, "A charge equalizer with a combination of APWM and PFM control based on a modified half-bridge converter," *IEEE Trans. Power Electron.*, vol. 31, no. 4, pp. 2970–2979, Apr. 2016.
[32] A. M. Imitiaz and F. H. Khan, "'Time shared flyback converter' based regenerative cell balancing technique for series connected Li-ion battery strings," *IEEE Trans. Power Electron.*, vol. 28, no. 12, pp. 5960–5975, Dec. 2013.
[33] M. Arias, J. Sebastián, M. Hernando, U. Viscarret, and I. Gil, "Practical application of the wave-trap concept in battery-cell equalizers," *IEEE Trans. Power Electron.*, vol. 30, no. 10, pp. 5616–5631, Oct. 2015.
[34] C.-S. Lim, K.-J. Lee, N.-J. Ku, D.-S. Hyun, and R.-Y. Kim, "A modularized equalization method based on magnetizing energy for a series-connected Lithium-ion battery string," *IEEE Trans. Power Electron.*, vol. 29, no. 4, pp. 1791–1799, Apr. 2014.
[35] Z. Zhang, H. Gui, D.-J. Gu, Y. Yang, and X. Ren, "A hierarchical active balancing architecture for lithium-ion batteries," *IEEE Trans. Power Electron.*, vol. 32, no. 4, pp. 2757–2768, Apr. 2017.
[36] S. Li, C. Mi, and M. Zhang, "A high-efficiency active battery-balancing circuit using multiwinding transformer," *IEEE Trans. Ind. Appl.*, vol. 49, no. 1, pp. 198–207, Jan. 2013.
[37] B. Poorali and E. Adib, "Analysis of the integrated SEPIC-flyback converter as a single-stage single-switch power-factor-correction LED driver," *IEEE Trans. Ind. Electron.*, vol. 63, no. 6, pp. 3562–3570, Jun. 2016.
[38] J.-P. Hong and G.-W. Moon, "A digitally controlled soft valley change technique for a flyback converter," *IEEE Trans. Ind. Electron.*, vol. 62, no. 2, pp. 966–971, Feb. 2015.
[39] R.-L. Lin and S.-H. Hsu, "Design and implementation of self-oscillating flyback converter with efficiency enhancement mechanisms," *IEEE Trans. Ind. Electron.*, vol. 62, no. 11, pp. 6955–6964, Nov. 2015.

Yunlong Shang (S'14) received the B.S. degree in automation from Hefei University of Technology, Hefei, China, in 2008. He is currently working toward the Ph.D. degree in the School of Control Science and Engineering, Shandong University, Shandong, China. In 2015, he received funding from China Scholarship Council and became a joint Ph.D. student in the Department of Electrical and Computer Engineering, San Diego State University, San Diego, CA, USA.

His current research interests include the design and control of battery management systems and battery equalizers, battery modeling, and battery state estimation.

Bing Xia (S'13) received the B.S. degree in mechanical engineering from the University of Michigan, Ann Arbor, MI, USA, and the B.S. degree in electrical engineering from Shanghai Jiaotong University, Shanghai, China, in 2012. He is currently working toward the joint Ph.D. degree at San Diego State University, San Diego, CA, USA, and the University of California, San Diego. He was a Ph.D. student in automotive system engineering at the University of Michigan Dearborn between winter 2013 and summer 2015.

His current research interests include batteries, including charging optimization, battery safety, and battery management.

Chenghui Zhang (M'14) received the Bachelor's and Master's degrees in automation engineering from Shandong University of Technology, Jinan, China, in 1985 and 1988, respectively, and the Ph.D. degree in control theory and operational research from Shandong University, Jinan, in 2001.

In 1988, he joined Shandong University, where he is currently a Professor in the School of Control Science and Engineering, the Chief Manager of the Power Electronic Energy-Saving Technology and Equipment Research Center of the Education Ministry, a Specially Invited Cheung Kong Scholars Professor of the China Ministry of Education, and a Taishan Scholar Special Adjunct Professor. He is also one of the state-level candidates of the "New Century National Hundred, Thousand and Ten Thousand Talent Project," the academic leader of the Innovation Team of the Ministry of Education, and the Chief Expert of the National "863" high technological planning. His current research interests include optimal control of engineering, power electronics and motor drives, energy-saving techniques, and time-delay systems.

Naxin Cui (M'14) received the B.S. degree in automation from Tianjin University, Tianjin, China, in 1989, and the M.S. and Ph.D. degrees in control theory and applications from Shandong University, Jinan, China, in 1994 and 2005, respectively.

In 1994, she joined Shandong University, where she is currently a Full Professor with the School of Control Science and Engineering. Her current research interests include power electronics, motor drives, automatic control theory and applications, and battery energy management systems of electric vehicles.

Jufeng Yang (S'15) received the B.S. degree in electrical engineering in 2012 from Nanjing University of Aeronautics and Astronautics, Nanjing, China, where he is currently working toward the Ph.D. degree (Master–Doctorate program) in electrical engineering. In 2015, he received funding from the China Scholarship Council and became a joint Ph.D. student in the Department of Electrical and Computer Engineering, San Diego State University, San Diego, CA, USA.

His current research interests include battery management systems, including battery modeling, battery model parameter identification, and battery state estimation.

Chunting Chris Mi (S'00–A'01–M'01–SM'03–F'12) received the B.S.E.E. and M.S.E.E. degrees in electrical engineering from Northwestern Polytechnical University, Xi'an, China, in 1985 and 1988, respectively, and the Ph.D. degree in electrical engineering from the University of Toronto, Toronto, ON, Canada, in 2001.

He is currently a Professor and Chair of Electrical and Computer Engineering and the Director of the Department of Energy (DOE)-funded Graduate Automotive Technology Education (GATE) Center for Electric Drive Transportation, San Diego State University, San Diego, CA, USA. From 2001 to 2015, he was with the University of Michigan, Dearborn, MI, USA. His current research interests include electric drives, power electronics, electric machines, renewable-energy systems, and electrical and hybrid vehicles. He has conducted extensive research and has published more than 100 journal papers.